Electronic Supplementary Material (ESI) for Journal of Materials Chemistry C.

Electronic Supporting Information

Charge transfer tuning in TiO_2 hybrid nanostructures with acceptor-acceptor systems

Kacper Pilarczyk, Kornelia Lewandowska, Krzysztof Mech, Michał Kawa, Marta Gajewska, Bolesław Barszcz, Andrzej Bogucki, Agnieszka Podborska, Konrad Szaciłowski**

*e-mails: podborsk@agh.edu.pl (Agnieszka Podborska), szacilow@agh.edu.pl (Konrad Szaciłowski)

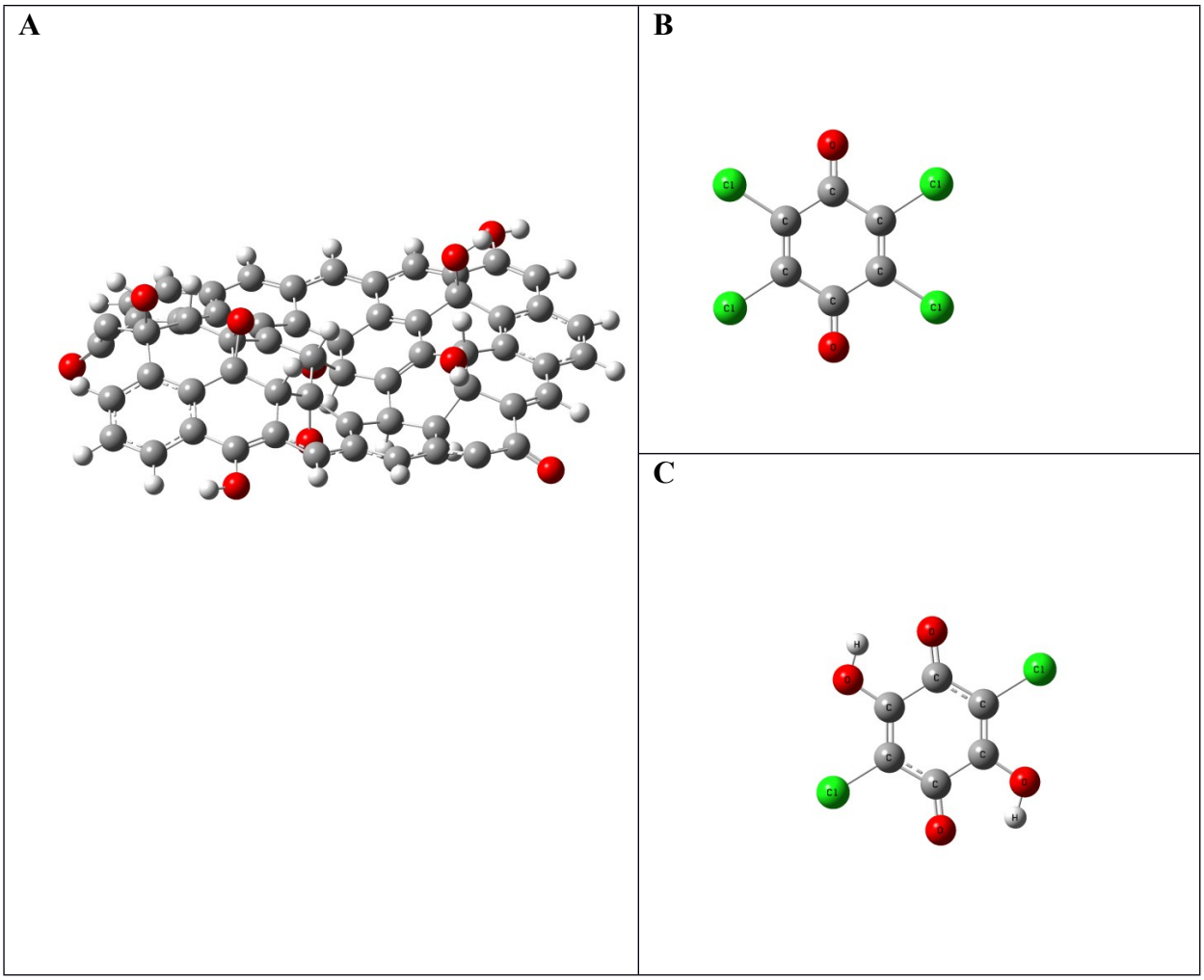

Scheme S1. The optimal configurations of GO (A), CLA (B) and KCLA (C).

Table S1. The calculated and experimental frequencies for CLA and CLA/GO dyad.

Theory (cm^{-1})	Raman (cm^{-1})		IR (cm^{-1})		Approximate description
CLA	CLA	CLA/GO	CLA	CLA/GO	
194	200	199			C-Cl scissoring
319	328	328			C-C-C bending (ring breathing)
491	494	494			C-C-Cl bending
695			713	713	C-Cl stretching
750			749	749	C-C-C bending out of plane
820	776	778			C-Cl stretching asymmetric (+ring deformation)
900			906	906	C-C-C scissoring
981	1006	1008			C-Cl stretching symmetric (+ring deformation)
1107			1111	1110	C-C stretching + C-Cl stretching
1232			1235	1235	C-C stretching
		1333			D band
1252	1246	1248			C-C stretching asymmetric
		1597			G band
1634			1647	1650	C=C stretching asymmetric
1667	1610 and 1691	1610 and 1691			C=C + C=O stretching symetric
1683			1680	1680	C=O stretching asymmetric

Table S2. The calculated and experimental frequencies for KCLA and KCLA/GO dyad.

Theory (cm^{-1})	Raman (cm^{-1})		IR (cm^{-1})		Approximate description
KCLA	KCLA	KCLA/GO	KCLA	KCLA/GO	
209	239				C-C-Cl rocking
285	287	282			Ring deformation
377	377	335			C-C-O bending
424	408	390			C-C-C bending
533	542				C-C-C bending
547					C-Cl stretching + ring deformation
617			636	636	C-C-C bending out of plane + C-C-O bending out of plane
704					O-H wagging
753			753	752	C-C-C bending out of plane
771	787				C-C-C bending out of plane
831			841	840	C-Cl stretching asymmetric
893	913				C-Cl stretching
977			980	980	C-C stretching asymmetric
1243	1244				C-Cl stretching + C-O-H bending + C-C stretching
1247			1270	1260	C-O-H bending + C-Cl stretching asymmetric
1269	1278				C-O stretching
1332			1362	1265	C-O-H bending + C-O stretching
		1333			D band
1375	1380				C-C stretching + C-O-H bending
		1597			G band
1647	1651				C=O stretching symmetric
1662			1666	1664	C=O stretching asymmetric
1711					C=C stretching asymmetric
1733	1675	1682			C=C stretching symmetric
3442			3304	3304	O-H stretching with hydrogen bonds

It is well established that the D band results from a breathing mode of κ-point photons of A_{1g} symmetry, while the G band arises due to the first order scattering of the E_{2g} phonons of sp^2 C atoms.[47] The most prominent bands in the CLA spectra may be related to the C=C bond stretching (1691 cm^{-1} and 1610 cm^{-1}) and C-C-Cl bond bending (494 cm^{-1}). There are also some less intensive bands which can be assigned to the specific vibrations of the CLA molecule. In the Raman spectrum of CLA/GO dyad we can identify those characteristic signals coming from CLA at almost the same Raman Shifts as in the case of pure CLA which indicates small or no interactions between CLA and GO. The presence of GO in CLA/GO system is confirmed by the appearance of the D band at 1333 cm^{-1} and the G band at around 1594 cm^{-1}. The G band is superimposed on the C=C stretching band at 1610 cm^{-1} so its position is less precisely defined. The Raman D/G intensity ratio (ID/IG) is proportional to the average size of sp^2 domains.[49] The CLA/GO has the same ID/IG value (1.20) as pure GO which is associated with the efficient protection of hydroxyl and epoxy groups in GO.

The experimental Raman spectra of pure KCLA agree relatively good with the calculation results. The most intensive bands are observed at 1651 cm^{-1} and 542 cm^{-1} and they are related to the C=O stretching and C-C-C bending vibrations, respectively. Less intensive signals can be also assigned to the specific vibrations within KCLA molecule (Table S2). The positions of the observed Raman lines are consistent with the results obtained by Pawlukojć et. al.[50], however the assignment of some bands to the specific vibrations is slightly different in our case. The spectrum of KCLA/GO dyad, when compared to the spectrum of pure KCLA, shows almost no bands except for the D and the G bands at 1333 and 1597 cm^{-1} originating from the GO vibrations. The Raman D/G intensity ratio (D/G) of KCLA/GO has a higher D/G value (2.21) compared to that of GO (1.14) and CLA/GO (1.20) suggesting

a partial restoration of the π-conjugated structures in the GO nanosheets or strong coupling between the π-orbitals of both partners. The additional bands observed in the spectrum recorded for KCLA/GO (after magnification by a factor of 20) at 282, 335 and 1682 cm^{-1} can be related to the vibrations within the KCLA molecule. However, if we compare the positions of those bands in the spectrum of KCLA/GO with those in the spectrum of pure KCLA we can notice that they are significantly shifted which indicates a stronger interaction between KCLA and GO than between CLA and GO.

The FT-IR spectrum obtained for GO exhibits typically observed stretching vibration peaks of O-H bands at approximately 3357 cm^{-1}, C=O at 1731 cm^{-1}, C-O-C at 1223 cm^{-1} and C-O at 1050 and approximately 1365 cm^{-1}.[1, 2] It is relatively easy to identify the bands characteristic for CLA vibrations in the spectrum of CLA/GO dyad. Similarly to the Raman spectra their positions are only slightly changed.

In the case of KCLA the significant differences between calculated and experimental spectra are noticed in the region of 1200-1400 cm^{-1} where the C-O-H bending vibrations are observed. This include some differences in intensities, width and number of bands. It is a clear suggestion that in a real material those bonds strongly interact with the environment. The simulated spectrum was calculated for an isolated molecule and all such interactions were neglected. This is probably the reason why we observe more signals in the experimental result. On the other hand, the bands recorded in this region by Pawlukojć et. al.[3] are also wider and more intense than calculated ones.

In the following paragraph we present data for organic compounds discussed in the manuscript, graphene oxide and dyads made of both aforementioned systems. The results include the UV-Vis absorbance spectra, the emission spectra and the deconvoluted Raman spectra in the range where the D and the G bands are recorded. The first two show no new interactions between GO and quinone derivatives. However, the thorough analysis of the latter reveals variations in the D/G ratio, which may be interpreted as an evidence for some interplay between both entities.

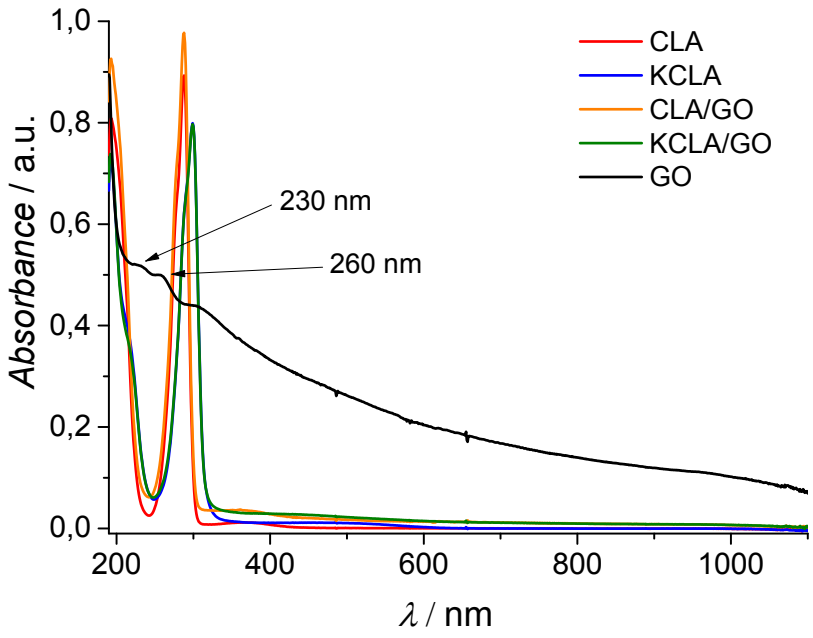

Fig. S1. The absorbance spectra of quinone derivatives, dyads with graphene oxide and GO without molecular modifier (in a higher concentration – refer to the experimental section). For clarity reasons the GO spectrum was multiplied by the factor of 2.

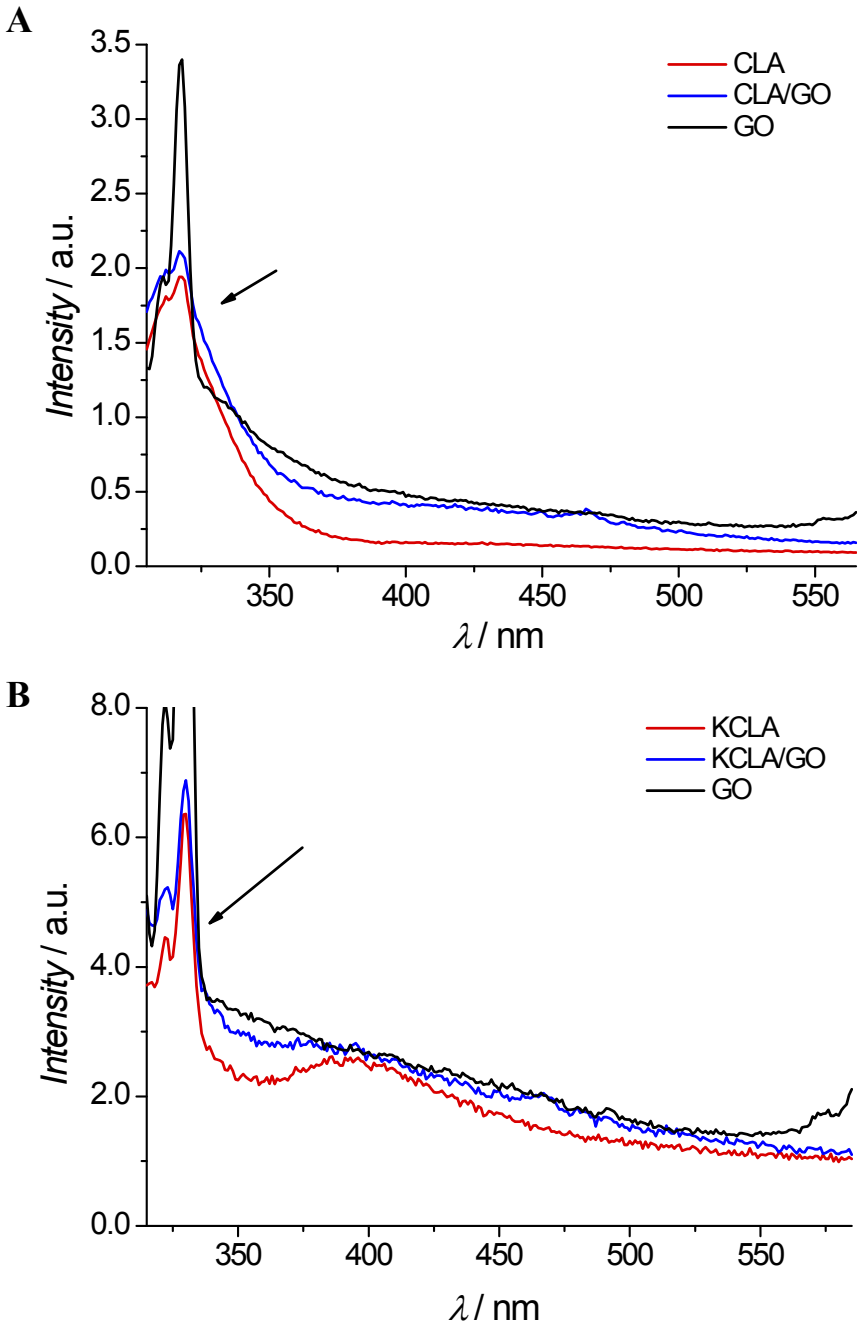

Fig. S2. The emission spectra of quinone derivatives, dyads with graphene oxide and GO in acetonitrile solution. The samples were excited at 290 nm (A) and 300 nm (B) which corresponds to the absorption peaks recorded for CLA and KCLA respectively.

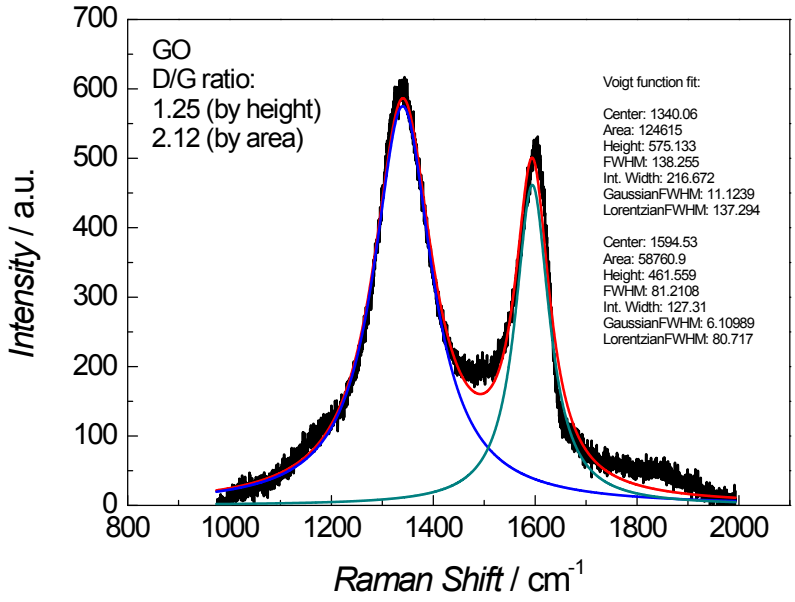

Fig. S3. The deconvolution done for the D and the G bands recorded in the Raman spectrum of GO sample.

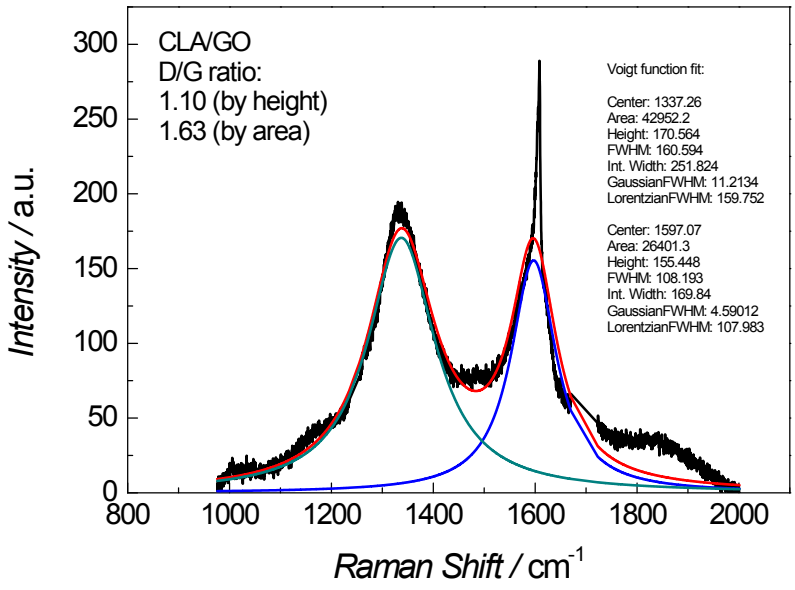

Fig. S4. The deconvolution done for the D and the G bands recorded in the Raman spectrum of CLA/GO sample.

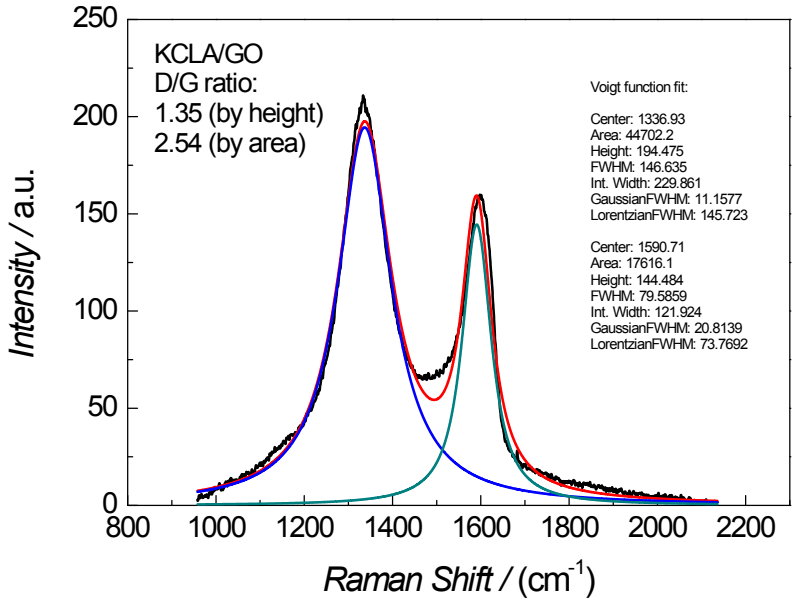

Fig. S5. The deconvolution done for the D and the G bands recorded in the Raman spectrum of KCLA/GO sample.

The morphology and the crystal structure of hybrids were investigated. In the next figure the X-ray diffractograms for titanium dioxide, cadmium sulphide and their composites with graphene oxide are presented. Authors postulated no significant changes in XRD patterns should emerge upon the addition of organic modifiers. One may notice a slight increase in the signal intensity at approximately 8° in the case of the GO/CdS system. That may be attributed to the presence of graphene oxide in the sample.

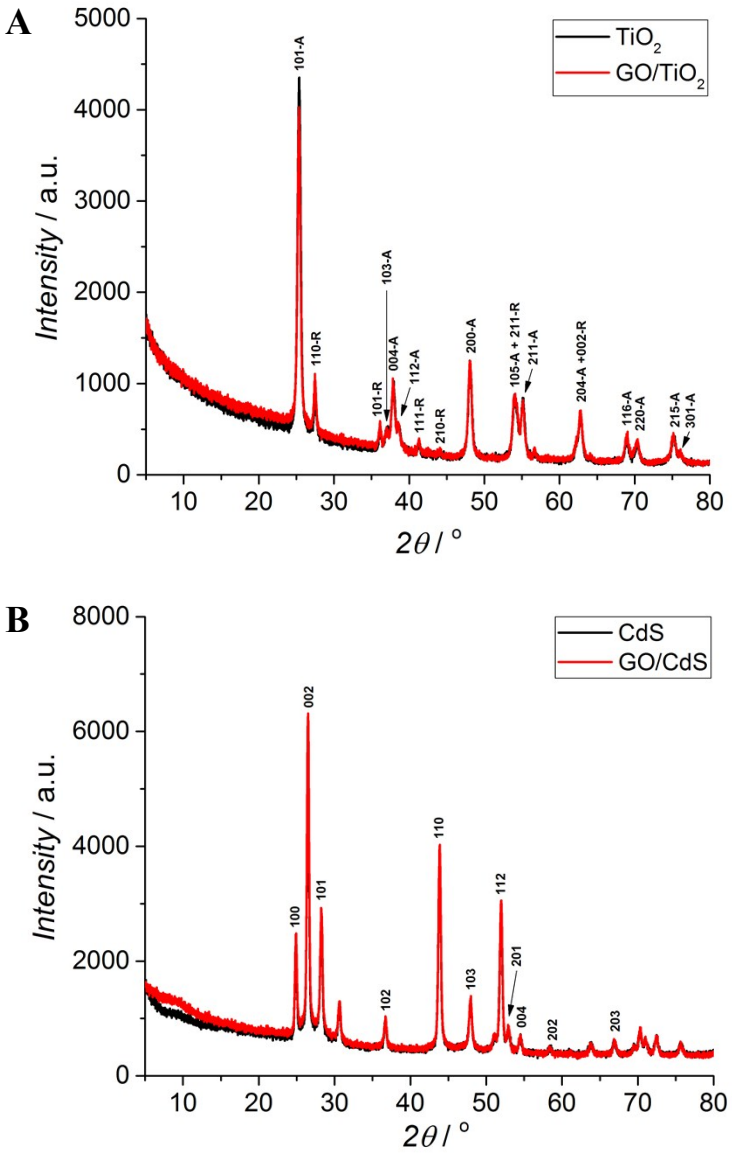

Fig. S6. The XRD patterns recorded for neat TiO_2, its hybrid with GO (A), neat CdS and its hybrid with GO (B).

We also demonstrate how the addition of various modifiers influences the reflectance and ATR-IR spectra recorded for cadmium sulphide-based hybrids. It seems that due to the electronic configuration of cadmium cations – $[Kr]4d^{10}$, whereas for titanium cations in TiO_2 the configuration can be described as $[Ar]3d^0$ – no strong coupling arise upon modification of CdS nanoparticles and the UV-Vis spectra are unaffected. At the same time, some minor variations

between IR spectra may be noticed – particularly for the CLA/CdS sample (a band at approx. 1560 cm^{-1} which can be attributed to the presence of CLA – cf. Figure 1 in the manuscript) – but they are irrelevant for the further analysis.

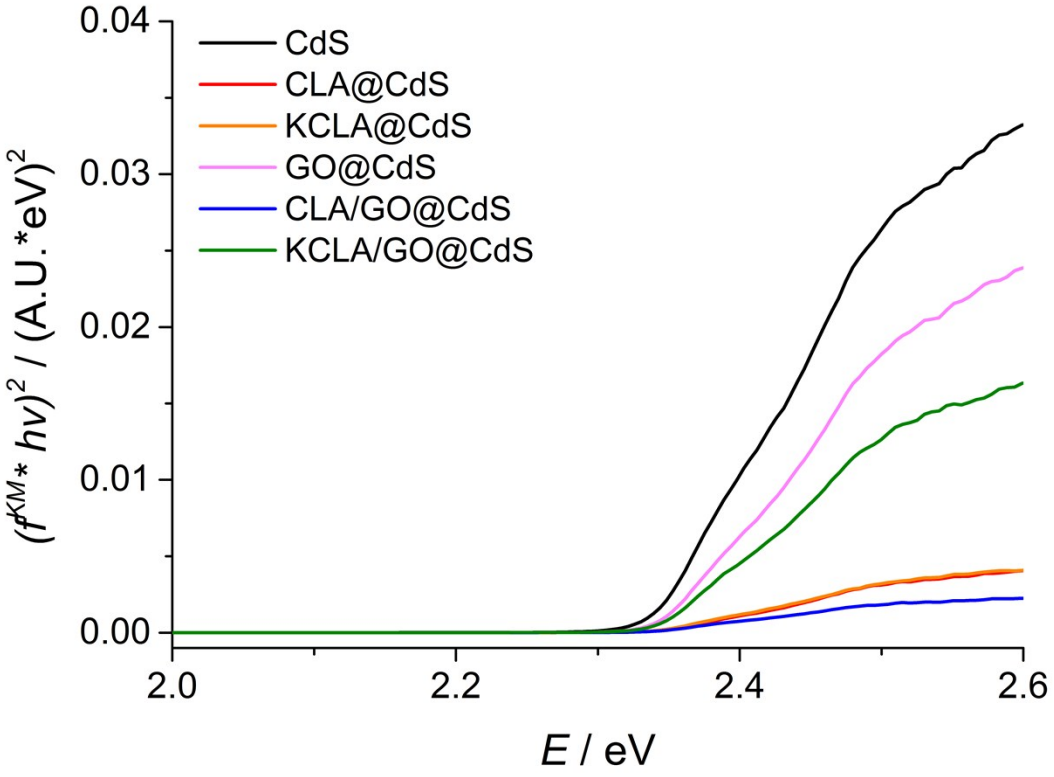

Fig. S7. The Tauc plots for cadmium sulphide and the hybrid materials containing CdS.

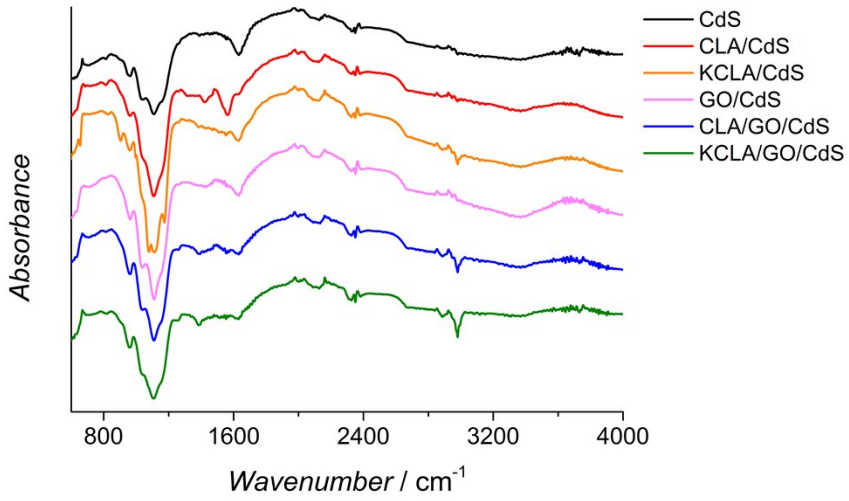

Fig. S8. The ATR-IR spectra of CdS hybrids with quinone derivatives, dyads with graphene oxide and GO deposited onto diamond crystal.

In the following section we present the photocurrent action spectra recorded for other systems and under various experimental conditions. The main goal is to show that the investigated oxides are almost completely unaffected by the presence of molecular oxygen in electrolyte. We would also like to point out that not only KCLA-based hybrids are strongly influenced by the addition of graphene oxide – the photocurrent response of CLA-containing materials also undergo some alterations. Finally, we wanted to present how other semiconductors (particularly other than oxides) are modified by the examined acceptor-acceptor dyads.

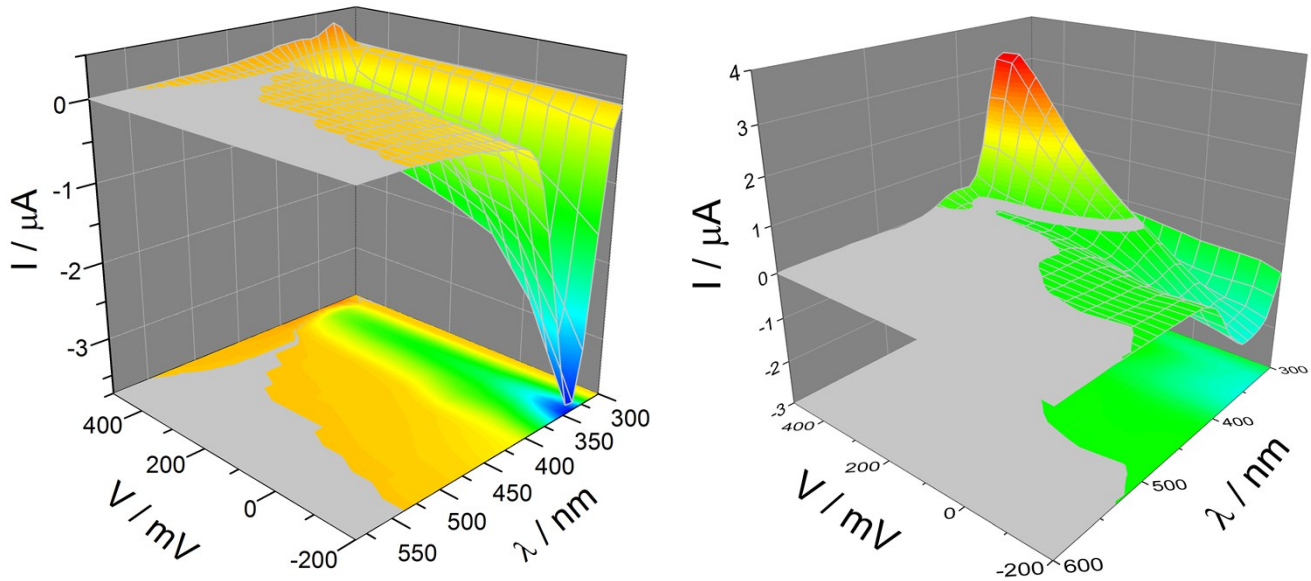

Fig. S9. The photocurrent action spectra recorded at different potential steps for TiO_2 modified with KCLA (left) or KCLA/GO dyadic modifier (right) in 0.1 M KNO_3 under O_2.

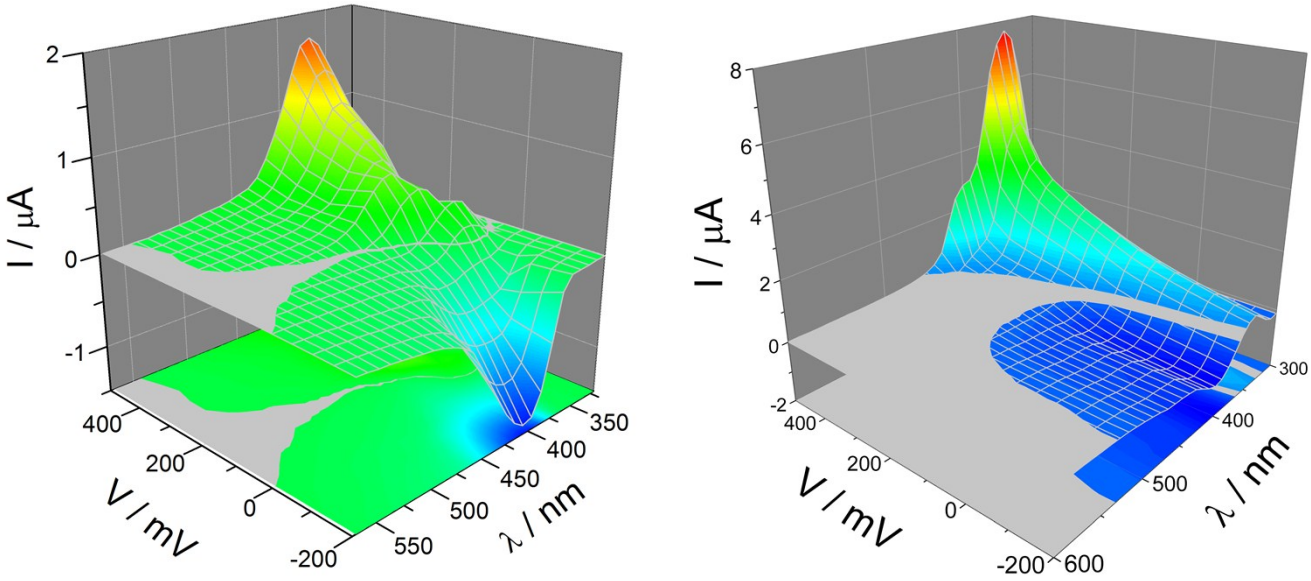

Fig. S10. The photocurrent action spectra recorded at different potential steps for TiO_2 modified with CLA (left) or CLA/GO dyadic modifier (right) in 0.1 M KNO_3 under Ar.

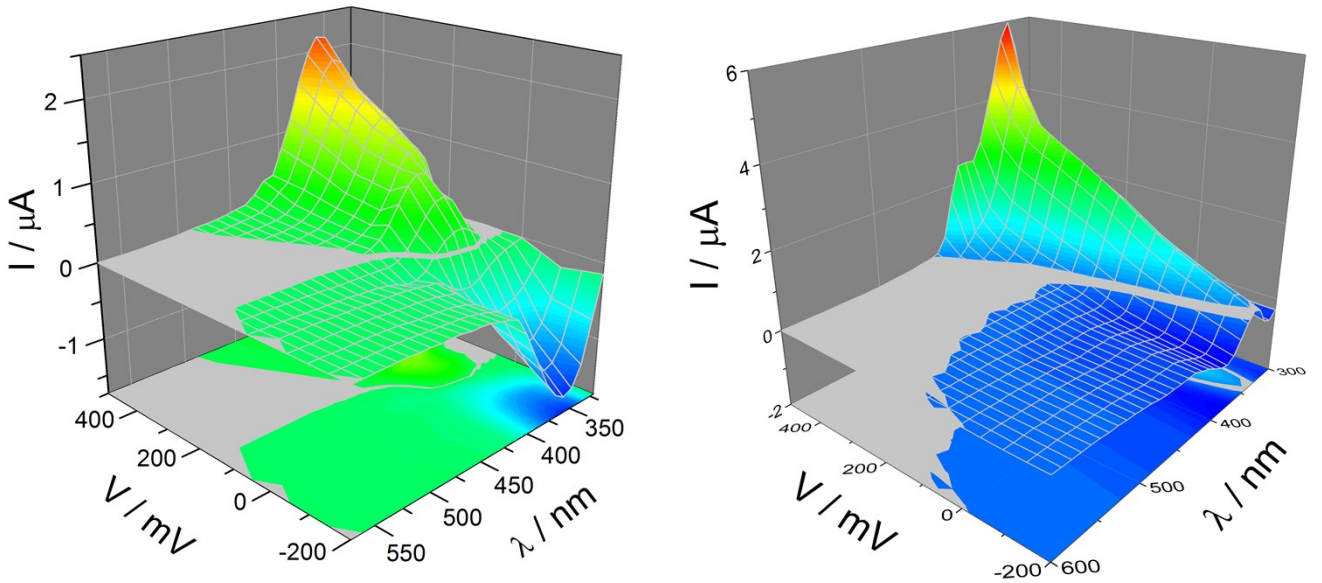

Fig. S11. The photocurrent action spectra recorded at different potential steps for TiO_2 modified with CLA (left) or CLA/GO dyadic modifier (right) in 0.1 M KNO_3 under O_2.

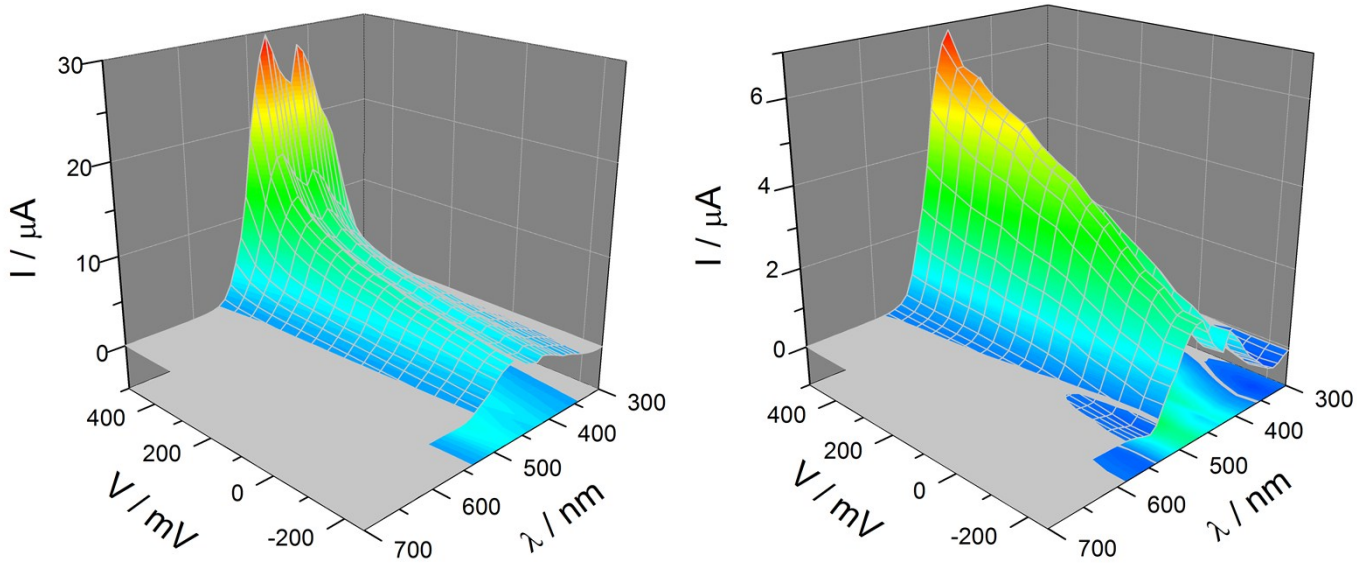

Fig. S12. The photocurrent action spectra recorded at different potential steps for CdS modified with KCLA (left) or KCLA/GO dyadic modifier (right) in 0.1 M KNO_3 under Ar.

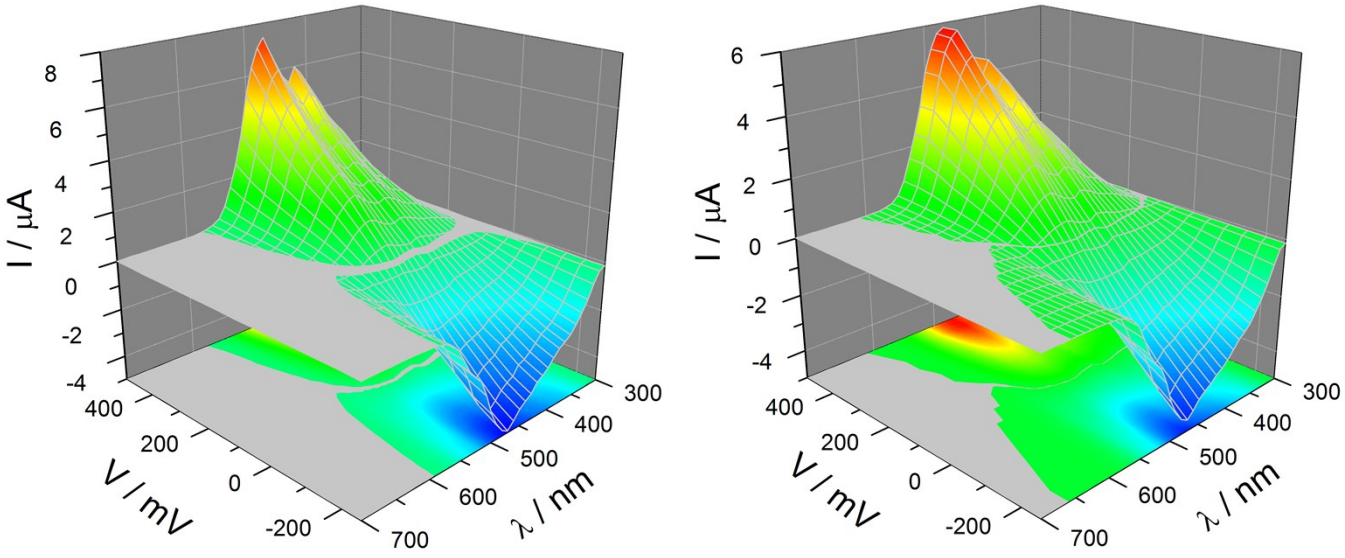

Fig. S13. The photocurrent action spectra recorded at different potential steps for CdS modified with KCLA (left) or KCLA/GO dyadic modifier (right) in 0.1 M KNO_3 under O_2.

The analysis of Fig. S12 and Fig. S13 reveals that cadmium sulphide is affected more by the presence of molecular oxygen in the experimental system than by the addition of graphene oxide. That may indicate a relatively weak interactions between this non-oxide semiconductor and the examined modifiers, probably due to the electronic configuration of cadmium cations and significantly lower concentration of oxygen-containing groups on the surface of CdS.

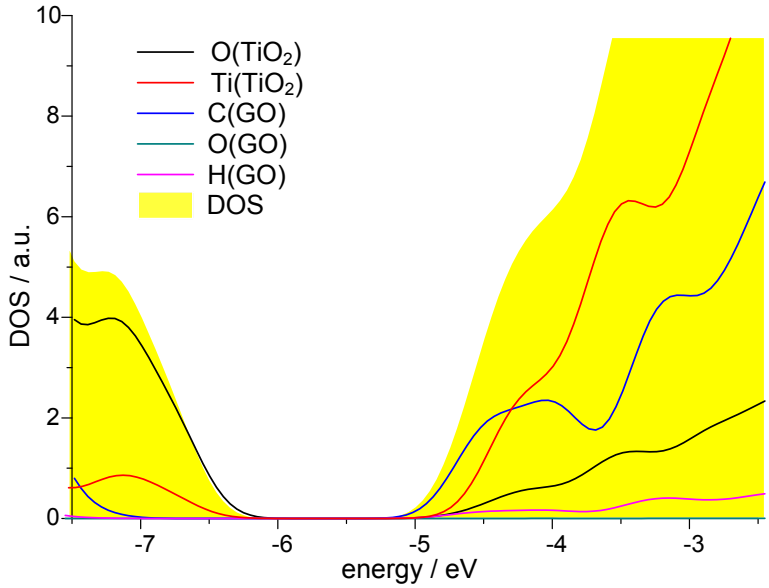

Figure S14. Density of states calculated for the TiO_2-graphene oxide hybrid of the stoichiometry $Ti_{56}O_{112}C_{260}O_{54}H_{40}$ at the PM7 level of theory with MOPAC2012, version 15.286W (yellow area). Lines represent projected density of states for corresponding fragments.

References

1. J. I. Paredes, S. Villar-Rodil, A. Martinez-Alonso and J. M. D. Tascon, *Langmuir* 2008, **24**, 10560–10564.
2. S. Stankovich, R. D. Piner, S. T. Nguyen and R. S. Ruoff, *Carbon*, 2006, **44**, 3342–3347.
3. A. Pawlukojc, G. Bator, L. Sobczyk, E. Grech and J. Nowicka-Scheibe, *J. Phys. Org. Chem.* , 2003, **16**, 709–714.